Pré-Publicações do Departamento de Matemática
Universidade de Coimbra
Preprint Number 23–06

RESPIRATORY PARTICLES: FROM ANALYTICAL ESTIMATES TO DISEASE TRANSMISSION

J. A. FERREIRA, P. DE OLIVEIRA AND P. SILVA

Abstract: Respiratory particles containing infectious pathogens are responsible for a large number of diseases. To define health politics and save lives, it is important to study their transmission mechanisms, namely the path of particles once expelled. This path depends on several driving factors as intrinsic properties of particles, environmental aspects and morphology of the scenario. Following physical arguments and taking into account the results of experimental works, we consider a mathematical drift model, where the mixture composed by two phases-air and particles- is viewed as a whole. The relative motion between the two phases is described by a kinematic constitutive relation. We prove the stability of the model for fixed times and establish an a priori estimate for the total number of infectious particles. The upper bound of this estimate exhibits sound physical dependencies on the driving factors, in agreement with the experimental literature. Namely, we confirm that the amount of particles expelled and their emission rate can explain why some people are superspreaders. Several numerical simulations illustrate the theoretical results.

AMS Subject Classification (2010): 35B45, 92B05, 65M60.

Keywords: Respiratory Particles, Evaporation, Settling, Partial Differential Equations, Drift model, Estimates, Numerical Simulation

1. Introduction

Biological Motivation

A large number of diseases are spread by respiratory particles, due to the possible presence of infectious pathogens, virus, bacteria or fungi, in their nuclei. These particles can be exhaled by all kind of respiratory events from breathing and talking, to the most violent ones as coughing and sneezing. In the last decades, the problem of air quality and airborne diseases transmission - as for example influenza, tuberculosis, measles or Covid-19 - drew the attention of a very large number of researchers working in different applied and experimental areas [5]-[26]. During Covid-19 pandemics the focus on the topic, essentially by researchers outside the field of mathematics, has hugely increased. The results produced had a crucial role in informing health politics and saving lives. We mention, without being exhaustive [4]-[16]. Our

Received February 24, 2022.

objective in this paper is to establish analytically those experimental results, from the study of a model based on a system of ordinary differential equations and a system of partial differential equations.

To achieve such a goal we must understand what happens to respiratory droplets once exhaled. After exhalation, the space-time evolution of respiratory droplets depends on several driving factors: properties of droplets, environmental factors and morphology of the scenario. Regarding these driving factors, we find several references in the literature as for example:

(i) Properties of droplets: amount, size, emission rate and viral load of exhaled particles [3], [4], [25];
(ii) Environmental factors: relative humidity (RH), temperature and ventilation [4], [19];
(iii) Morphology of the scenario: obstacles and materials [1], [13], [26].

We proceed to make some comments about those factors. The droplet radii, measured in different experimental works (for example [25]) are reported to range in the interval $[0.5, 1000]$ where the units are micrometers (μm). However around 95% have radii in the interval $[1, 60]$. This size distribution appears largely independent of the type of respiratory event. On the contrary, the number of exhaled droplets depends mainly on the type of respiratory event: a few thousand for a cough, up to a million for a sneeze. The fate of respiratory droplets, emitted by an infected person during a respiratory event is different for "large" and "small" particles. The definition of "small" and "large" is based on experimental results and the radius size cut-off has variations from study to study. Currently the World Health Organization guidelines define this cut-off at 5 μm. "Large" particles fall on available deposition surfaces, within a short time, and can produce contamination by direct contact; "small" particles stay suspended in the air for longer periods and can be inhaled by other people in the same space ([3]). This type of contamination is called airborne transmission. Regarding environmental factors, laboratorial results suggest that temperature and relative humidity influence the persistence of a large number of virus as is the case of SARS-CoV-2. Temperature increases the decay of enveloped viruses. However, as our focus in this paper is airborne contamination in indoor spaces, we assume that the indoor temperature is regulated and consequently that the main environmental driver of transmission is RH. In fact RH influences the fate of respiratory particles for two different reasons. Firstly, low RH accelerates evaporation, reduces the radius of particles and consequently their weight,

what makes them stay suspended in the air longer. Secondly, RH governs the survival of pathogens inside the droplets. The relation between RH and virus inactivation rate is a complex one represented by an U- shaped function, for a large number of virus ([1]). As what concerns ventilation, different systems can be considered from passive to forced ventilation. With reference to the morphology of the scenario, several aspects could be considered as deposition on the vertical walls, on the floor, or on the furniture. To keep the model as simple as possible, while taking into account the main phenomena involved, we will use a simplified description of deposition based on a global deposition rate ([1]). Figure 1 shows a diagram of the main factors governing the trajectory of respiratory particles.

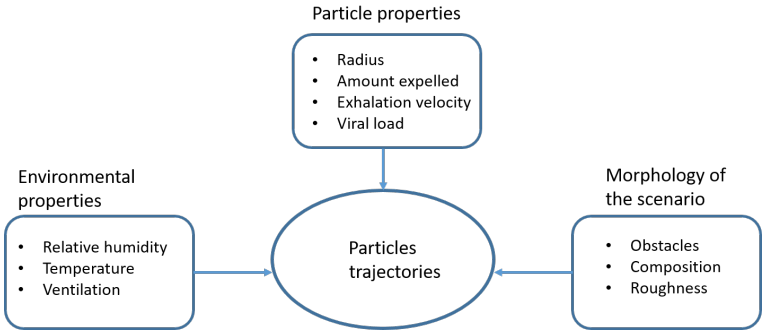

FIGURE 1. The space-time evolution of respiratory particles depends on several driving factors.

What is the interplay between those factors? Particles are expelled from the respiratory system, dispersed in the air and the water vapor flow. Once expelled, particles enter unsaturated air, travel under the action of convection, diffusion and gravity. They start to evaporate and the radius decreases: the largest particles are deposed on available surfaces and the smallest particles stay suspended in the air. The amount by which a particle radius decreases depends on its initial radius, the fraction of non volatile matter in the droplet nuclei-including pathogens, sugars, proteins, lipids - and on the relative humidity in the domain ([26]). As the radius shrinks, the droplet loses water vapor, and its density increases because nuclei are denser than the water vapor where they are entrapped: the higher RH, the lower is the evaporation rate (Figure 2).

Mathematical models in the literature

The flow of respiratory droplets suspended in the air can be considered a two-phase disperse flow. To model disperse flows, two main approaches

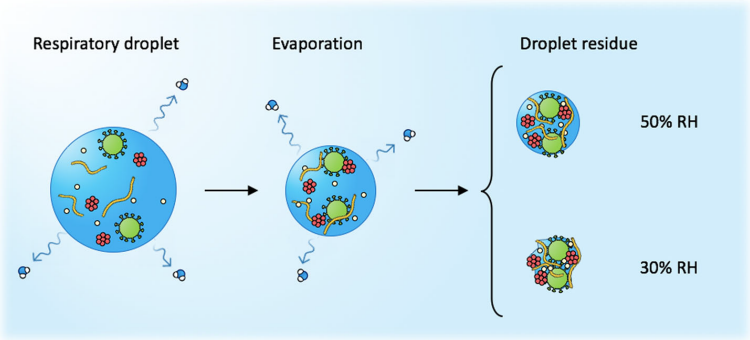

FIGURE 2. Particles and non-volatile nuclei: the influence of RH ([4]).

can be found in the literature: trajectory models and two-fluid models. In the trajectory models, the motion of the disperse phase - the particles - is governed by Newton's second law, taking into account gravity, buoyancy, drag force and the force responsible for the momentum destruction of vapour due to evaporation. The models based on this physical description, are described by two coupled ordinary differential equations (ODE) for each particle. One of the equations is used to compute the velocity and the other to define the position occupied by the particle ([3], [6], [21]-[23]). The ODE systems for the velocity u_p and the position s of a particle, with a certain initial radius, are of the form

$$\begin{cases} \dfrac{d\,(m_p u_p)}{dt} = F_g + F_b + F_d + F_s \\ \dfrac{ds}{dt} = u_p, \end{cases} \tag{1}$$

where m_p represents the time-dependent mass of the particle, F_g stands for the gravity force, F_b represents the buoyancy, F_d the drag force and F_s represents the force responsible for the momentum destruction of vapour due to evaporation. System (1) is closed with initial conditions for u and s. Regarding trajectory models, we mention without being exhaustive, a number of formulations based on system (1), found in the literature and progressively more realistic:

(i) The simplest description considers that after leaving the exhaled flow the respiratory droplets move in a static indoor air, following a ballistic trajectory ([6]). The path of large droplets is dominated by gravity while the trajectories of small droplets can remain longer suspended in the air, leading to a greater dissemination. This means that large droplets tend to fall in seconds, depositing on surfaces and

small droplets can travel for a longer period, being eventually inhaled by someone else. The conclusions are qualitatively in agreement with experimental results.

(ii) The experimental set up in [3] and [23] suggests that the path of particles is influenced by the respiratory flow. Following this rationale, system (1) was modified by including in the drag force F_d a velocity for the expelled air: an empiric velocity ([23]), or a velocity described by Navier-Stokes equations ([20] and [21]).

(iii) In a third type of trajectory models found in the literature, the fluid flow behavior of droplets is modelled using two different systems, one for large and the other for small droplets. For large droplets it is used Newton's Law, where the velocity of the expelled air is computed by Navier-Stokes equations as in (ii); however the path of single small particles is omitted and it is identified with the fluid flow governed by Navier-Stokes and mass transfer equations ([15], [20]).

The second approach found in the literature, to describe disperse flows, is two fluid models, where the discrete nature of particles is overlooked and the disperse phase is treated as a continuous phase. In this approach, conservation equations are developed for the two flows, which presents many difficulties related to the interactions between the two phases ([12]). A simplified version of two-fluid models are drift-flux models where the mixture is considered as a whole, rather than two separate phases. The formulation involves two mass conservation equations, one for each phase, and one momentum equation for the mixture. The mass conservation of the dispersed phase is modelled by using a drift equation, that includes the relative velocity between the phases. The approach is largely used in the literature (for example [5], [8], [26], [27]) and the simulations presented therein are in agreement with experimental results ([13], [15], [17]). Specifically, the model has been validated for indoor particle dissemination ([13]).

The present contribution

In the present paper, we are interested in indoor propagation of respiratory particles possibly leading to airborne contamination. We adopt a drift-flux model and our focus is the study of mathematical aspects related to theoretical estimates. Namely, we want to analyse if, from these theoretical estimates, it is possible to conclude the type of dependence on the driving factors, established by experimentalists.

The topic of airborne contamination has always attracted the attention of a very large number of researchers from applied areas, contributing with laboratorial results or numerical simulations. We believe that our approach represents an original contribution as it shows that the mathematical analysis of a priori estimates exhibits sound physical properties, leading to results in line with laboratory experiments.

The paper is structured as follows. In Section 2 we establish the equations, following the principles of drift-flux models for disperse flows. The stability of the mathematical model is then deduced in Section 3. An a priori estimate of the total number of particles highlights the relative weight of the different driving factors, and supports a number of health guidelines adopted to block disease spread. The estimates are numerically illustrated and compared with results in the experimental literature. In Section 4 several numerical experiments are presented. In Section 5 some conclusions are addressed.

2. Mathematical model

In this section we present the mathematical model that describes the evolution of the number density of respiratory droplets exhaled indoors, during a violent respiratory event - coughing or sneezing. It is assumed that particles are laden with virus and that evaporation takes place after expulsion. Moreover we assume that ventilation is guaranteed by a passive system.

We consider a drift-flux model ([5], [8], [10], [12]) where the mixture composed by two phases - air and particles - is viewed as a whole and the relative motion between the two phases is described by a kinematic constitutive relation.

2.1. Convection-diffusion-reaction equation for the dispersed phase.

Let $\Omega \subset \mathbb{R}^2$ represents the physical domain where the evolution of respiratory droplets is studied. Let the boundary $\partial\Omega$ be decomposed in

$$\partial\Omega = \partial\Omega_W \cup \partial\Omega_D \cup \partial\Omega_F \cup \partial\Omega_{w_a} \cup \partial\Omega_{M_f} \cup \partial\Omega_{M_b}$$

as represented in Figure 3. The boundaries $\partial\Omega_W$ and $\partial\Omega_D$ represent two openings of a passive ventilation system, a window and a door respectively; $\partial\Omega_F$ stands for the floor of the room. Ω_M stands for the location of the emission source and its boundary satisfies $\partial\Omega_M = \partial\Omega_{M_f} \cup \partial\Omega_{M_b}$, where $\partial\Omega_{M_f}$ represents the entry of the respiratory flow in Ω. Finally $\partial\Omega_{w_a}$ represents the remaining boundaries.

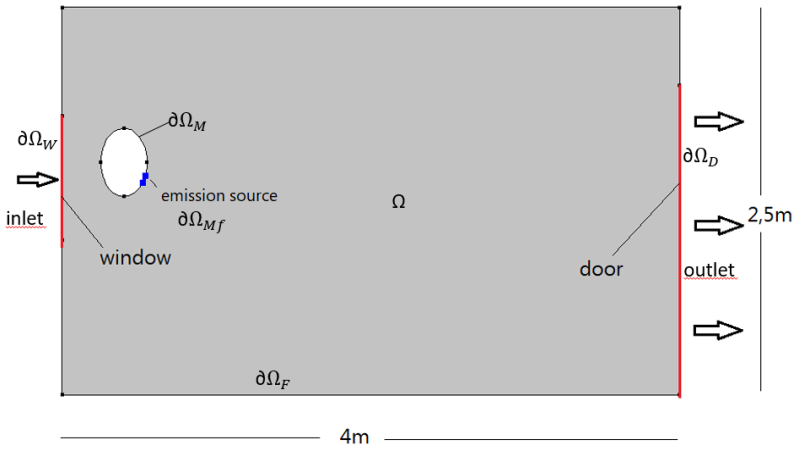

FIGURE 3. A vertical slice of the domain.

We consider an arbitrary reference domain $A \subseteq \Omega$. The respiratory particles are assumed spherical with radius $R(t)$ and density $\rho_p(t)$. We suppose that evaporation takes place as the particles are expelled, which explains that radius and density are time dependent. We also assume that particles, while evaporating, keep their spherical shape. To guarantee that the particles can be considered in the continuum regime and that the usual equations of continuum mechanics can be applied, we assume that the Knudsen number, k_n, satisfies $k_n \ll 1$. As $k_n = \frac{\lambda}{R(t)}$, where λ is the mean free path of air molecules, we obtain $R_0 \gg 0.0651\,\mu m$ ([9]) and consequently the continuum regime can be used for particles with radii exceeding this value.

Let $C(x,t)$ stand for the number density of respiratory particles with infectious nuclei and with initial radius R_0, in $x \in \Omega$ at time t. The total mass of particles, with infectious nuclei and with initial radius R_0, in A is given by

$$M(t) = \int_A m_p(t)\, C(x,t)\, dx, \tag{2}$$

where $m_p(t)$ represents the mass of a particle, that is defined by $m_p(t) = \frac{4}{3}\pi R^3(t)\rho_p(t)$. The variation of $M(t)$ in A is due to the flux J that crosses the boundary ∂A of A, to the deposition, to the inactivation of pathogens and the loss of mass by evaporation. J is a convection-diffusion flux that will be

defined later in this paper. To take into account these phenomena we write

$$\begin{aligned} M'(t) = & -\int_{\partial A} m_p(t)J(x,t).\eta\, ds - \int_A m_p(t)KC(x,t)\, dx \\ & -\int_A m_p(t)VC(x,t)\, dx - \int_A m_p(t)L(t)C(x,t)\, dx. \end{aligned} \tag{3}$$

The sinks of the model, K and V, stand for the deposition of particles and the inactivation rate of the pathogens, respectively. The deposition of particles K, defined later in this section, is represented by a global deposition rate depending on several parameters. Regarding the inactivation rate V, we focus on its dependence on relative humidity. It is represented, for most virus, by an U-shaped function. In Figure 4 is exhibited a plot of the inactivation rate of SARS-CoV-2 as a function of RH. In equation (3), η stands for the exterior unit normal.

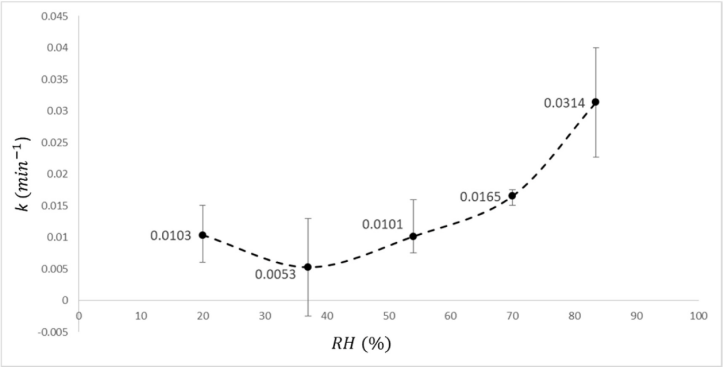

FIGURE 4. Inactivation rate of SARS-CoV-2 as a function of RH ([1]).

As already mentioned in Section 1, we assume that, indoors, the temperature is regulated and that the inactivation rate depends essentially on relative humidity ([1], [19]). In the last term of the second member of equation (3), that quantifies mass loss by evaporation, the time function $L = L(t)$ stands for the rate of evaporation.

From equation (2) and equation (3) we have

$$m_p\frac{\partial C}{\partial t} + \frac{dm_p}{dt}C = -m_p div(J) - m_pKC - m_pVC - m_pLC, \tag{4}$$

where we omitted the time and space variables. We recall that C and J are space-time functions, m_p and L are time functions, K and V are constants depending on several parameters.

Let us assume that the droplets don't evaporate completely, that is $m_p(t) \neq 0$, $\forall t \in [0, T_e]$. This assertion will be justified in what follows.

As $m_p'(t) < 0$, the rate of evaporation L can be defined by

$$L(t) = -\frac{m_p'}{m_p} \tag{5}$$

and we deduce from equations (4) and (5) that the number density of particles with infectious nuclei satisfies

$$\frac{\partial C}{\partial t} = -div(J) - (K + V)C \text{ in } \Omega \times (0, T_e]. \tag{6}$$

The emission of virus laden particles is represented by a boundary condition active on $\partial\Omega_{M_f}$ as the respiratory event lasts (Figure 3).

2.2. Particle radius and density: the effect of evaporation. Let us justify that is an acceptable physical assumption to consider $m_p(t) \neq 0$, $\forall t \in [0, T_e]$.

Following for example [26], [4] and [18], the evolution of $R(t)$ can be described, in a simplified form, by

$$R(t) = \begin{cases} R_0(1 - \dfrac{\theta(1 - RH)t}{R_0^2})^{\frac{1}{2}}, t \leq t_{ev} \\ R_0(\dfrac{\phi_0}{1 - RH})^{\frac{1}{3}}, t > t_{ev}. \end{cases} \tag{7}$$

In equation (7), R_0 is the initial radius of the particle, θ is a physical parameter ([4]) and RH represents relative humidity. Respiratory particles are liquid droplets that contain non-volatile nuclei, composed by sugars, proteins, lipids and pathogens. The typical volume proportion of the non volatile content, ϕ_0, satisfies

$$1\% \leq \phi_0 \leq 10\%,$$

and a dried particle devoid of water has a radius $R_0(\frac{\phi_0}{1-RH})^{\frac{1}{3}}$ ([4]). The previous arguments justify that $R(t) \neq 0$, for every t and consequently that $m_p(t) \neq 0$ in $(0, T_e]$. The evaporation time, t_{ev}, is obtained from equations (7) by assuming continuity of $R(t)$.

As the radius $R(t)$ shrinks the density of the particles, $\rho_p(t)$, increases because the nuclei are denser than the evaporating water (Figure 2). Assuming

that particles keep a spherical shape, while evaporating, we have

$$\rho_p(t) = \begin{cases} 1 + (\rho_p^n - 1)\dfrac{R_0^3\phi_0}{R^3(t)(1-RH)}, t \leq t_{ev} \\ \rho_p^n, t > t_{ev}, \end{cases} \tag{8}$$

where ρ_p^n is the density of the non-volatile nuclei, that is the final density of the particle. The expression for $\rho_p(t)$ for $t \leq t_{ev}$ is easily deduced from

$$\rho_p(t) = \frac{(R^3(t) - R_0^3\phi_0^*) + R_0^3\phi_0^*\rho_p^n}{R^3(t)}, \tag{9}$$

where $\phi_0^* = \phi_0/(1-RH)$. Values for ρ_p^n depend on the nuclei composition and can be found in experimental studies. For example for Sars-Cov-2 a density of $1.3\, g/ml$ is suggested in [22].

We illustrate the time behaviour of R, ρ_p and m_p in Figure 5 for $R_0 = 60$ microns and $RH = 0.5$. It can be observed that R and m_p are decreasing functions and ρ_p is an increasing function of time.

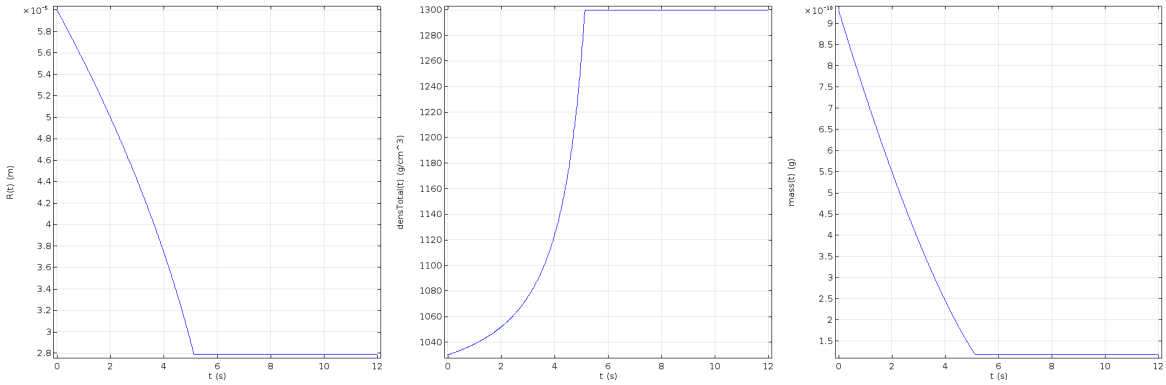

FIGURE 5. Plots of $R(t)$, $\rho_p(t)$ and $m_p(t)$ during 12 seconds.

2.3. The drift flux model. In the present paper we use a drift-flux model ([8], [10]). The principles underlying this class of models are the following:

1. One momentum equation is established for the mixture;
2. Conservation of mass is established for the two phases;
3. Relative motion of the particles, with respect to airflow, is essentially due to the gravitational settling of the dispersed phase.

The mixture momentum equation and the mass conservation for the airflow are given by

$$\begin{cases} \dfrac{\partial(\rho_f u_f)}{\partial t} + \nabla.(\rho_f u_f) = \nabla.(\mu_{eff}\nabla u_f) - \nabla p \\ \nabla.(\rho_f u_f) = 0, \qquad \text{in } \Omega \times (0, T_e], \end{cases} \tag{10}$$

where u_f is the air flow velocity, ρ_f stands for air density, μ_{eff} represents the effective diffusion and p represents the pressure. We observe that a simplification is made, when considering that ρ_f represents air density and not the mixture density. The approximation is justified by the small volume of respiratory particles when compared with the air volume in Ω.

Following principle 3, the velocity field u, that represents the velocity of particles, is defined as $u = u_f + u_{pf}$, where u_{pf} is the relative velocity of particles with respect to airflow that is defined as the settling velocity, u_s ([26], [27]), given by the steady state solution of system (1), which equation we will deduce in what follows.

From equation (6) we can conclude that mass conservation of evaporating particles, with non-volatile nuclei, is equivalent to a convection-diffusion-reaction equation for the density number of particles that reads

$$\frac{\partial C}{\partial t} + \nabla.((u_f + u_s)C) = \nabla.(D\nabla C) - (K + V)C \text{ in } \Omega \times (0, T_e]. \tag{11}$$

In (11), D represents a diffusion coefficient. For high Reynolds number of the flow, Re, $D = D_B + \epsilon$, where D_B is the Brownian diffusion and ϵ is the eddy diffusivity ([26]).

To compute the settling velocity of the particle, u_s, let us now return to system (1). As F_s, the force responsible for the moment destruction of vapor due to evaporation, is defined by $-m_p'(t)u_p(t)$, we have from (1)

$$m_p u_p' = F_g + F_b + F_d, \tag{12}$$

where the gravity force, F_g, the buoyancy, F_b, and the drag force, F_d, are defined respectively by

$$\begin{cases} F_g = \dfrac{4}{3}\pi R^3 g\rho_p, \\ F_b = -\dfrac{4}{3}\pi R^3 g\rho_f, \\ F_d = \dfrac{1}{2}C_d\rho_f\pi R^2\|u_f - u_p\|_{[L^2]^2}(u_f - u_p), \end{cases} \tag{13}$$

In (13), $\|.\|_{[L^2]^2}$ denotes the usual norm in $L^2(\Omega) \times L^2(\Omega)$, R and ρ_p are time functions that represent the particle's radius and density respectively, $g = (0, 0, -9.8)$ and C_d is the drag coefficient defined by ([6])

$$C_d = \frac{21.12}{Re_p} + \frac{6.3}{\sqrt{Re_p}} + 0.25. \tag{14}$$

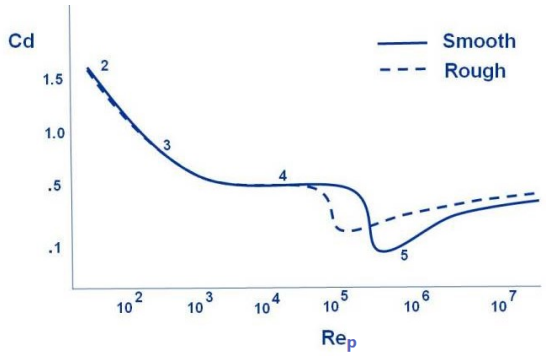

FIGURE 6. The behaviour of the drag constant C_D as a function of Re_p . Image from https://www.grc.nasa.gov/www/k-12/airplane/dragsphere.html.

Equation (14) represents an empirical relation that holds for particles with Reynolds number, Re_p, such that $0.2 < Re_p < 2 \times 10^3$. We define ([23])

$$Re_p = \frac{2\rho_f R(t)\|u_f(t) - u_p(t)\|_{[L^2]^2}}{\upsilon}, \tag{15}$$

where υ is the kinematic viscosity of air. As Re_p is not constant because radius and velocity are time dependent, we illustrate in Table I, the maximum value of the Reynolds number for particles with initial radii $R_0 = 1\,\mu m$ and $R_0 = 60\,\mu m$ for a constant norm of the velocity of expelled particles $(10m/s)$, where the air is considered static. We select these two values of R_0 as representative of expelled particles because around 95% of these particles have radii that stay in the interval $[1, 60]$.

Table I: Maximum value of particle's Reynolds number (Re_p).

R_0 (μm)	Max Re_p
1	2.688
60	80.6

The settling velocity, u_s, is the steady solution of (12), (13) under quiescent conditions, that is when $u_f = 0$ ([27]). We obtain

$$|u_s| = \sqrt{\frac{8|g|R_0(\frac{\phi_0}{1-RH})^{\frac{1}{3}}(\rho_p^n - \rho_f)}{3C_d^*\rho_f}}. \tag{16}$$

In (16), $|.|$ denotes the euclidian norm for vectors, C_d^* is the value of the drag coefficient C_d corresponding to the steady state. The velocity u_s has the same direction as gravity: it points downward, perpendicularly. As the particle's Reynolds number at the steady state is defined by $2R_0(\phi_0^*)^{1/3}|u_s|/v$, the exact settling velocity can be calculated only iteratively from (16). For the purposes of the theoretical estimates presented in Section 3, we circumvent such difficulty, by using superior and inferior bounds for C_d^*, computed from the assumption that of the particle's Reynolds number satisfies $0.2 < Re_p < 2\times 10^3$. That is, if $Re_{min} < Re_p < Re_{max}$ then

$$C_{d,min} < C_d^* < C_{d,max}, \tag{17}$$

where $C_{d,i}, i = min, max$, is calculated from (14) with a Reynolds number Re_i, $i = max$, min.

2.4. Initial and Boundary Conditions. The boundary conditions of the model are defined by:

- for the velocity u_f (defined by (10))

$$\begin{cases} u_f = u_w \text{ on } \partial\Omega_W \times (0, T_e], \\ u_f = u_{f_{in}} \text{ on } \partial\Omega_{M_f} \times (0, T_e], \end{cases} \tag{18}$$

  and a no-slip boundary condition for u_f on $(\partial\Omega \setminus (\partial\Omega_W \cup \partial\Omega_{M_f})) \times (0, T_e]$. In equation (18), u_w represents the passive ventilation velocity and $u_{f_{in}}$ stands for the velocity of the respiratory airflow.
- for the concentration C

$$\begin{cases} J.\eta = \alpha_W C \text{ on } \partial\Omega_W \times (0, T_e] \\ J.\eta = \alpha_D C \text{ on } \partial\Omega_D \times (0, T_e] \\ J.\eta = 0 \text{ on } \partial\Omega_F \times (0, T_e] \\ J.\eta = 0 \text{ on } (\partial\Omega_{w_a} \cup \partial\Omega_{M_b}) \times (0, T_e] \\ J.\eta = -\dfrac{E(t)}{|\partial\Omega_{M_f}|} \text{ on } \partial\Omega_{M_f} \times (0, t_d] \\ J.\eta = 0 \text{ on } \partial\Omega_{M_f} \times (t_d, T_e], \end{cases} \tag{19}$$

  where $J = -D\nabla C + C(u_f + u_s)$, t_d is the duration of the respiratory event, E represents the number of particles emitted by time unit and

$|\partial\Omega_{M_f}|$ stands for the measure of $\partial\Omega_{M_f}$. The rate constants α_W and α_D are positive.

Null initial conditions are assumed for the velocity u_f and for the total number of particles per volume unit, C.

3. Qualitative behaviour

An energy estimate that proves the stability of the model for finite times is presented in this section. An expression for the total number of particles is also established. An upper bound of this expression depends on a number of parameters that characterize the driving factors (Figure 1).The qualitative behaviour of this estimate leads to results in agreement with experimental literature.

We begin by establishing an energy estimate for the concentration C. Multiplying equation (11) by C and taking the integral in Ω we have

$$\frac{1}{2}\frac{d}{dt}\|C\|^2 + \int_\Omega \nabla.((u_f + u_s)C)C\,dx = \int_\Omega \nabla.(D\nabla C)C\,dx - S\|C\|^2, \quad (20)$$

where the sink S is defined by

$$S = K + V, \quad (21)$$

and $\|.\|$ denotes the usual norm in $L^2(\Omega)$. In (21), V represents the inactivation rate of the pathogen and K represents a global deposition rate, defined in ([1]) by

$$K = \frac{|u_s|}{|H|}, \quad (22)$$

where u_s stands for the perpendicular settling velocity computed from (16), and $|H|$ is the height of the emission source. We recall the u_s points downward perpendicularly. From (16), (21) and (22) we deduce that S is defined by

$$S(RH, R_0) = \Big[\frac{8}{3}\frac{R_0}{C_D^*}\Big(\frac{\phi_0}{1-RH}\Big)^{1/3}|g|\frac{\rho_p^n - \rho_f}{\rho_f}\Big]^{\frac{1}{2}}\frac{1}{|H|} + V, \quad (23)$$

where the dependence of S on RH and R_0 is explicited. In (23), C_D^* represents the drag coefficient corresponding to the steady state of system (12).

As

$$\int_\Omega \nabla.((u_f + u_s)C)C\,dx = -\int_\Omega (u_f + u_s)C.\nabla C\,dx + \int_{\partial\Omega}(u_f + u_s).\eta C^2\,d\omega,$$

and

$$\int_\Omega \nabla.(D\nabla C)C\,dx = -\int_\Omega D\|\nabla C\|^2_{[L^2]^2}\,dx + \int_{\partial\Omega} DC\nabla C.\eta\,d\omega,$$

from (20) we have

$$\frac{1}{2}\frac{d}{dt}\|C\|^2 = -D\|\nabla C\|^2_{[L^2]^2} + \int_\Omega (u_f+u_s)C.\nabla C\,dx + \int_{\partial\Omega} CJ.\eta\,dw - S\|C\|^2. \tag{24}$$

Assuming that $u_f(t)+u_s \in [L^\infty(\Omega)]^2$, we have from (24)

$$\frac{d}{dt}\|C\|^2 + (2D-\epsilon^2)\|\nabla C\|^2_{[L^2]^2} - h(t)\|C\|^2 + 2\sum_{i=W,D}\alpha_i\|C\|^2_{L^2(\partial\Omega_i)} \\ -2\int_{\partial\Omega_{M_f}} \frac{E(t)}{|\partial\Omega_{M_f}|}C\,d\omega < 0, t\in(0,T_e], \tag{25}$$

where $\epsilon \neq 0$ is an arbitrary constant. In equation (25), $h(t) = \dfrac{\|u_f(t)+u_s\|_{[L^\infty(\Omega)]^2}}{\epsilon^2} - 2S(RH,R_0)$ and $E(t)=0, t>t_d$, where t_d stands for the duration of the respiratory event.

The last integral term in the first member of (25) satisfies

$$2\int_{\partial\Omega_{M_f}} \frac{E(t)}{|\partial\Omega_{M_f}|}Cd\omega \leq \frac{1}{\delta^2}\frac{1}{|\partial\Omega_{M_f}|}E^2(t) + \delta^2\|C\|^2_{L^2(\partial\Omega_{M_f})}, \tag{26}$$

where $\delta\neq 0$ and for $\Gamma\subseteq\partial\Omega$, $\|.\|_{L^2(\Gamma)}$ denotes the usual norm is $L^2(\Gamma)$.

Replacing (26) in (24) we obtain

$$\frac{d}{dt}\|C\|^2 + (2D-\epsilon^2-\delta^2)\|\nabla C\|^2_{[L^2]^2} - (h(t)+\delta^2K_T)\|C\|^2 \leq -2\sum_{i=W,D}\alpha_i\|C\|^2_{L^2(\partial\Omega_i)} \\ +\frac{1}{\delta^2}\frac{1}{|\partial\Omega_{M_f}|}E^2(t), \tag{27}$$

where K_T is a constant resulting from the application of a Trace Theorem ([7]) to $\|C\|^2_{L^2(\partial\Omega_{M_f})}$. Selecting ϵ and δ such that $2D-\epsilon^2-\delta^2K_T>0$ we establish

$$\|C\|^2 \leq \int_0^t e^{\int_s^t (h(\mu)+\delta^2 K_T)d\mu} \frac{1}{\delta^2} \frac{1}{|\partial\Omega_{M_f}|} E^2(s)ds, \ t \in [0, T_e], \tag{28}$$

and

$$\|C\|^2 \leq \int_0^t e^{-2S(RH,R_0)(t-s)} e^{\int_s^t (\|u_f(\mu)+u_s\|_{[L^\infty]^2}+\delta^2 K_T)d\mu} \frac{1}{\delta^2} \frac{1}{|\partial\Omega_{M_f}|} E^2(s)ds. \tag{29}$$

Inequality (29) proves the stability, for fixed time T_e, of the initial boundary value problem defined by equation (11) with the boundary conditions (19).

Let us now estimate the total number of respiratory particles in the room.

The total number of respiratory particles in suspended in the air with initial radius R_0, N, is represented by $\int_\Omega C dx$. Integrating the two members of equation (11) in Ω, we have

$$N'(t) = \int_{\partial\Omega} -J.\eta \, d\omega - S(RH, R_0)N(t). \tag{30}$$

Computing then a solution of (30) we have

$$N(t) = \int_0^t e^{-S(RH,R_0)(t-s)} \Big[E(s) - \sum_{i=W,D} \alpha_i \int_{\partial\Omega_i} C \, d\omega \Big] ds. \tag{31}$$

As $\alpha_i \geq 0$, $i = W, D$, from (17) and (31) we conclude

$$N(t) \leq \int_0^t e^{-S(RH,R_0)(t-s)} E(s)ds, \tag{32}$$

where in $S(RH, R_0)$, C_d^* is replaced by $C_{d,max}$.

From (23) and (32) we can establish the following conclusions:

(1) $N(t)$ is a decreasing function of the initial radius R_0. The conclusion has a sound physical meaning because large droplets deposit first and consequently are not suspended in the air ([6]). The plots in Figure 8 and 9 illustrate the result.

(2) $N(t)$ is a decreasing function of RH, the relative humidity. Higher is RH, lower is the evaporation rate and therefore particles, fall first to the floor, and consequently are not suspended in the air ([4]). This result is illustrated in Figure 10.

(3) The total number of particles $N(t)$ increases with $\hat{E}$, that is the total number of particles emitted during the event. The result is illustrated in Figure 11 and shows why large emissions characterize super-spreader's events. The increase of $N(t)$ with the rate of exhalation, defined in (18), can be established from (29). However, for the parameters used in the numerical simulations, the influence of $u_{f_{in}}$ is not meaningful (Figure 12).

4. Numerical illustrations

The problem is solved in the two-dimensional geometry represented in Figure 3, using Comsol Multiphysics software. A quadratic piecewise finite element method for the concentration equation is considered. A triangular mesh automatically generated with 40957 elements is used to obtain a consistent mesh. We note that for the conditions considered in the numerical simulations presented in this section, the Reynolds number of the airflow does not exceed 2600. The time integration is performed with a backward difference method, with variable order ranging between 1 and 2 and an adaptative time step. To compute the numerical solutions of the Navier-Stokes equations and of the concentration equation, streamline diffusion and crosswind diffusion stabilizers were used in both equations.

The values used for the parameters in the numerical simulations are presented in Table II.

Table II: Variables and parameters used in the simulations

Variable/Parameter	Value	Unit	Description
m_p		g	mass of a particle
C		n/m^3	number density of particles
K		$1/s$	deposition rate
V	0.01, 0.017	$1/s$	inactivation rate
J		$n/(m^2 s)$	convection diffusion flux
R_0	2, 60	μm	initial radius
ϕ_0	0.1	-	percent of non volatile content
RH	0.5, 0.7	-	relative humidity
t_{ev}		s	evaporation time
ρ_p^n	998.6	Kg/m^3	nucleus density
D	1.8×10^{-5}	m^2/s	diffusion coefficient
ρ_f	1.2077	Kg/m^3	fluid density
μ	1.488×10^{-5}	m^2/s	effective viscosity
p		P	pressure
g	9.8	m/s^2	gravity acceleration
C_d			drag coefficient
u_s		m/s	settling velocity of the particles
$u_{f_{in}}$		m/s	inlet velocity profile ([11]) - cough event
u_w		m/s	velocity of room passive ventilation
α_W, α_D	0.01	m/s	transfer coefficient - particle's flux

Convergence tests have been carried out with meshes of decreasing size to verify that the solution is mesh independent. In Table III we present the relative errors for the concentrations considering a reference solution obtained with a mesh with 51997 elements in $[0, 10]$. We observe that an increase in the number of elements leads to a decreasing of the relative error. An increase of 3.75 times of the number of elements leads to a decrease in the relative error of 68 times for $t = 5$, of 132 times at $t = 7$ and of 325 times for $t = 10$.

Table III: Relative error with respect to the L_∞ norm at t=5, 7 and 10.

Number of elements	$t = 5$	$t = 7$	$t = 10$
10931	0.34	0.66	1.30
22417	0.13	0.25	0.46
30799	0.127	0.22	0.37
40957	0.005	0.005	0.004

The problem is solved for small and large particles with two initial representative radius of 2 and 60 microns (μm), respectively. To simulate a respiratory event of cough, the velocity profile $u_{f_{in}}$ presented in Figure 7 is considered ([11]). The maximum velocity considered is $10.5\, m/s$ and the event lasts for 0.5 seconds.

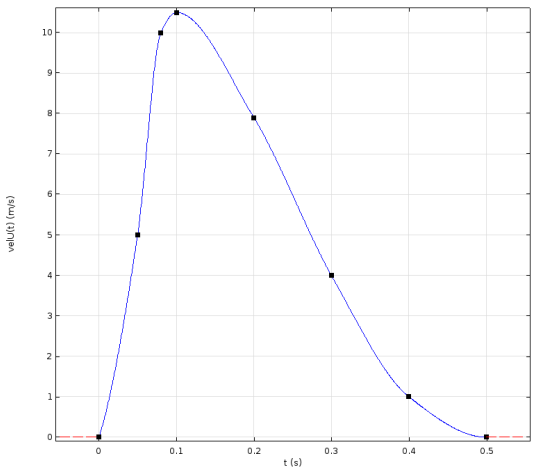

FIGURE 7. Inlet velocity profile $|u_{f_{in}}|$, for a cough event, defined on the boundary of $\partial\Omega_{M_f}$ ([11]).

In order to study the differences between the paths of large and small particles, when a slight ventilation rate is considered ($|u_w| = 0.1$), we exhibit in Figure 8 the dependence of the total number of particles $N(t)$, on the initial radius R_0, during 10 seconds for $R_0 = 2$ and $R_0 = 60$ μm with $RH = 0.5$. We note that $N(t)$ is a decreasing function of R_0: large particles deposit first and don't contribute to airborne dissemination.

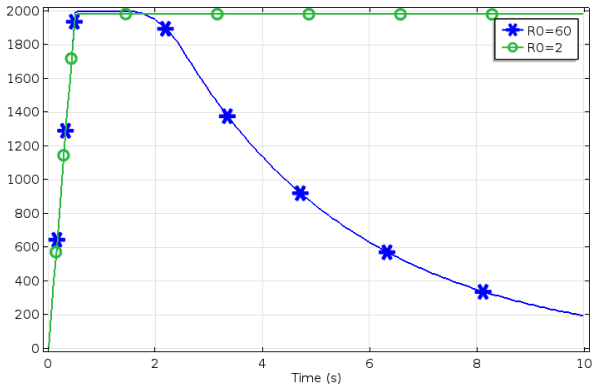

FIGURE 8. The dependence of $N(t)$ on R_0 during 10 seconds with $RH = 0.5$.

To get a clearer view of the dependence of $N(t)$ on R_0 we exhibit in Figure 9 the space-time evolution of particle distribution for $R_0 = 2, 60$ at $t = 0.5, 1, 3$. These plots were obtained from the results in Figure 8. We note that, as expected, deposition is more significant for large particles. In addition large particles hit the floor at $0.5m$; instead small particles remain essentially suspended in the air. These simulations suggest that for large

particles the guidelines for a two meters social distancing, adopted by the World Health Organization, during Covid-19 pandemic, prevents the spread of disease. However for small particles this social distancing is not enough.

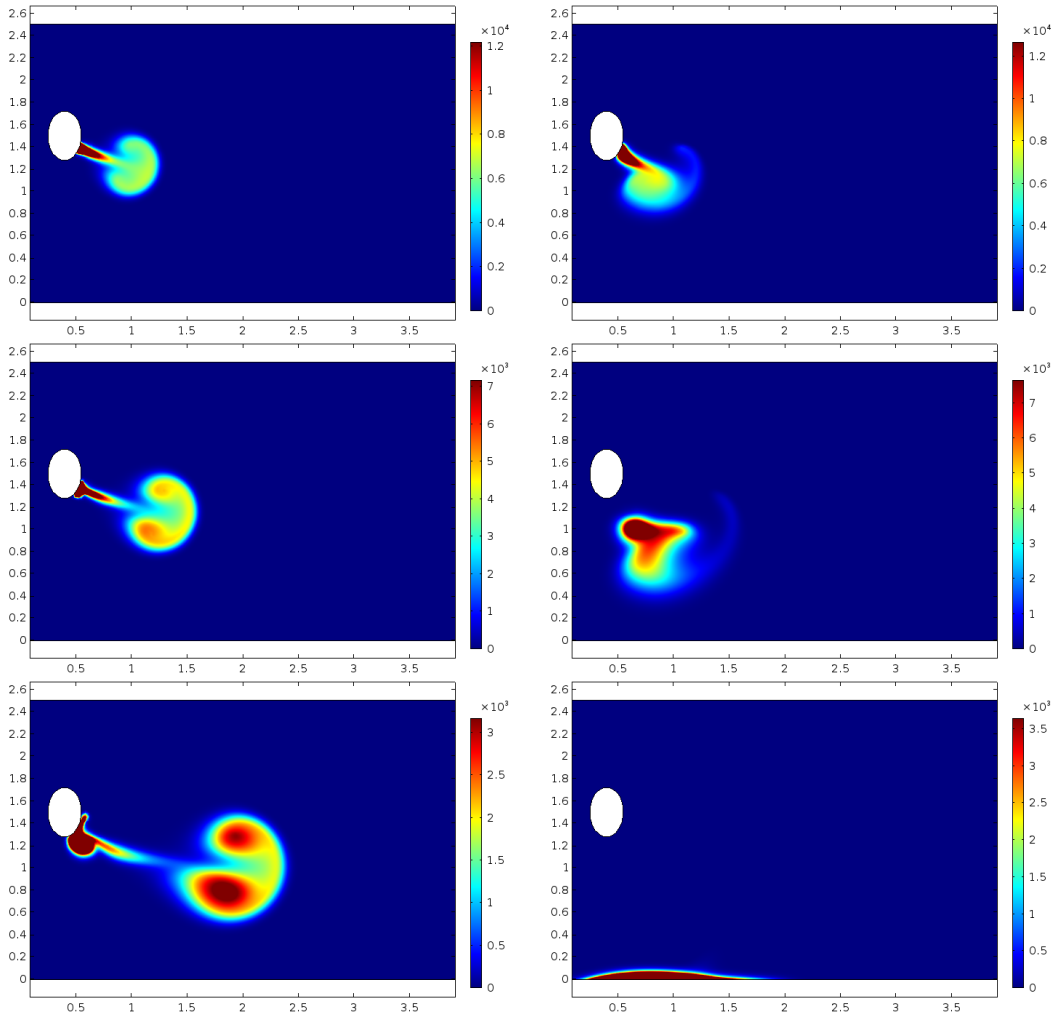

FIGURE 9. The effect of R_0 on the concentration distribution at $t = 0.5, 1, 3$, $|u_w| = 0.1$, $RH = 0.5$: small particles $R_0 = 2$ - left, large particles $R_0 = 60$ - right.

In what follows the dependence of $N(t)$ on the relative humidity RH, the total emission E and the velocity of room passive ventilation u_w are illustrated. As mentioned in Section 2 the numerical plots, in Figures 8, 9, 10 and 11, confirm the theoretical results deduced from estimate (32). The reference values considered for the fixed parameters are $R_0 = 60$, $u_w = 0$, $RH = 0.5$ and an emission particles per unit time , $E = 4000$. The global

number of particles emitted during an event that lasts $t_d = 0.5$, is 2000 as represented in the plots.

In Figure 10 the influence of relative humidity for small ($R_0 = 2$) and large particles ($R_0 = 60$) is illustrated with slight ventilation ($u_w = 0.1$). We observe that an increase in the relative humidity implies a decrease in the number of suspended particles in the room and that the influence of humidity is more significant in the case of heavy particles. The decay of the number of particles is larger in this case.

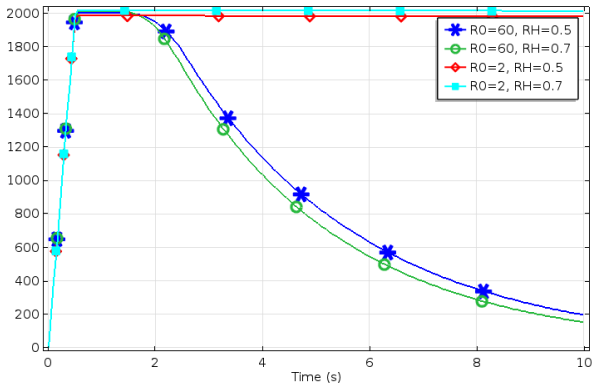

FIGURE 10. Influence of RH on $N(t)$ for small ($R_0 = 2$) and large ($R_0 = 60$) particles during 10 seconds.

The effect on $N(t)$, of the number of particles emitted per time unit, during 10 seconds is plotted in Figure 11 for $\hat{E} = 4000$, $\hat{E} = 8000$ and $t_d = 0.5$. As expected, the larger the emitting source, the greater the number of particles in the room.

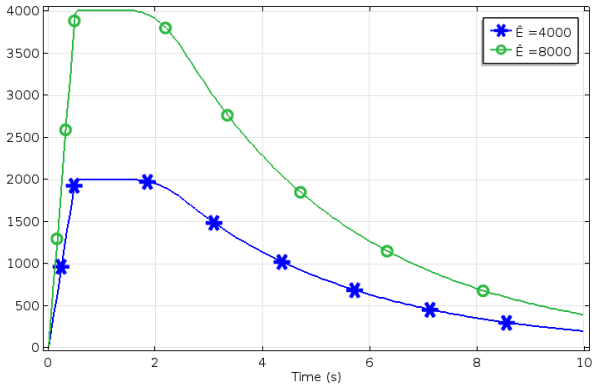

FIGURE 11. Influence of the number of particles emitted, on $N(t)$ during 10 seconds ($R_0 = 60$, $RH = 0.5$, $t_d = 0.5$).

In Figure 12 it is illustrated the influence of the velocity of the expired flow (18), $u_{f_{in}}$, defined on the boundary of $\partial\Omega_{M_f}$. An increase in the expiration rate leads to a very slight increase of $N(t)$ during the two first seconds. We observe that the expiration velocity acts only during the duration of the event, $t_d = 0.5$, what can explain the very slight influence.

In some indoors respiratory events a single infected person, called a super-spreader, is more likely to infect other people. Different reasons are invoked to explain these super-spreader events. We begin by mentioning biological reasons as a greater number of expelled particles, $\hat{E}$, and higher rates of emission $E(t)$ ([2]). The plot in Figure 11 confirm this hypothesis.

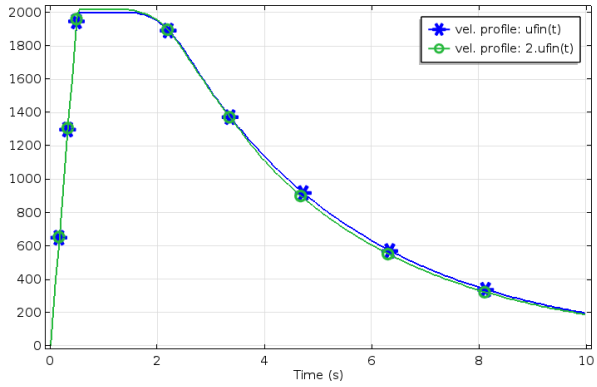

FIGURE 12. The influence of the inlet velocity on $N(t)$.

Another common feature of indoor super-spreader events is poor ventilation ([24]). The dependence of $N(t)$ on the ventilation, for small and large particles, is illustrated in Figure 13 for $|u_w| = 0.1, 2$ over 10 seconds, for $R_0 = 2$ on the left and $R_0 = 60$ on the right ($RH = 0.5$). Ventilation keeps small particles suspended, preventing them from deposition; the larger is $|u_w|$ the longer they stay suspended. After an initial period, the particles arrive at the door and leave the room. As particles transported by a ventilation with $|u_w| = 2$ arrive first, this can explain why after 10 seconds, in a well ventilated room there are no more particles. However it is a sound physical hypothesis that α_D increases with u_w. This assumption would have confirmed the recommendations by health authorities, for efficient natural ventilation. Regarding large particles, deposition is dominant; consequently as it does not depend on u_w, the difference is less significant. Notwithstanding this difference can be again explained by the fact that particles transported by an initial ventilation of $|u_w| = 2$ get to the door first. The plots in Figure 13

confirm the recommendations by health authorities, for an efficient natural ventilation.

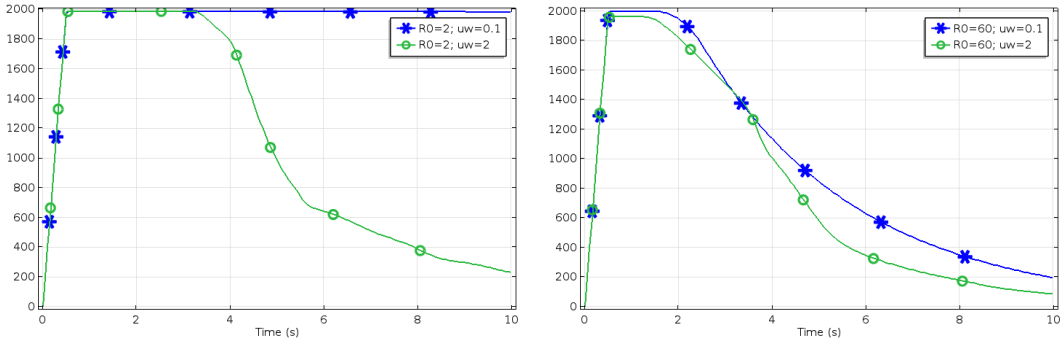

FIGURE 13. The effect of ventilation on $N(t)$ over 10 seconds ($R_0 = 2$ on the left; $R_0 = 60$ on the right).

5. Final Remarks

Inhaling indoor air is the primary mean by which people is exposed to respiratory particles. Knowledge of the trajectory of respiratory particles is essential to support the definition of guidelines that minimize airborne transmission of diseases.The study of the trajectory of respiratory particles is complex because it depends on a large number of phenomena and factors. As with all mathematical models, it is important to keep the description of phenomena as simple as possible, but exhibiting the main properties established by physical laws. Based on several laboratorial studies we focus on a small number of factors, related to intrinsic particle properties - initial radius and expelling velocity - and environmental properties - relative humidity.

We summarize in what follows the main conclusions established from the estimates, regarding the total number of airborne particles:

- The total number of airborne particles increases with the number of particles emitted per time unit $E(t)$ and with the total number of particles emitted, $\hat{E}$. This conclusion is in agreement with the hypothesis of some researchers, that a small percent of people are responsible for a large number of infections. In fact researchers believe that, among other biological causes, this could be a consequence of individuals - the superspreaders - that emit a higher number of particles per time unit. The plots in Figure 11 illustrate this influence.
- The total number of airborne particles decreases with RH. This conclusion is in agreement with a number of experimental studies ([19],

[4]) and suggests an explanation for the seasonality of respiratory infections. The rationale under this explanation is that in winter people spends more time indoor, with warmer temperatures, that dry the air coming from outdoors, which leads to a drop in RH. This causes a large evaporation rate and consequently a higher number of suspended respiratory particles. The numerical plots in Figure 10 illustrate the influence of RH.

- The total number of airborne particles is a decreasing function of the initial radius R_0. The conclusion has a sound physical meaning because large droplets deposit first and consequently are not suspended in the air ([3], [6]). The plot in Figure 8 illustrates the result.
- Ventilation reduces the number of respiratory particles indoors. The plots in Figure 13 confirm the recommendations of health authorities regarding ventilation.

Despite its simplicity, the model allows establishing results in accordance with laboratory work.

Acknowledgments

This work was partially supported by the Centre for Mathematics of the University of Coimbra - UIDB/00324/2020, funded by the Portuguese Government through FCT/MCTES.

References

[1] A. Aganovic, Y. Bib, G. Cao, F. Drangsholt, J. Kurnitski, P. Wargocki, Estimating the impact of indoor relative humidity on SARS-CoV-2 airborne transmission risk using a new modification of the Wells-Riley model, Building and Environment, 205 (2021), 108-278.

[2] S. Asadi, A. S. Wexler, C. D. Cappa, S. Barreda, N. M. Bouvier, W. D. Ristenpart. Aerosol emission and superemission during human speech increase with voice loudness. Scientific Reports, 9:2348 (2019), 1-10.

[3] L. Bourouiba, E. Dehandschoewercker, J. W. M. Bush, Violent expiratory events: on coughing and sneezing, Journal of Fluid Mechanics, 745 (2014), 537-563.

[4] A. Bozic, M. Kanduc, Relative humidity in droplet and airborne transmission of disease, Journal of Biological Physics, 47(2021), 1-29.

[5] F. Chen, C.M. Simon, A.C.K. Lai, Modeling particle distribution and deposition in indoor environments with a new drift-flux model, Atmospheric Environment, 40 (2006), 357-367.

[6] C. H. Cheng, C. L. Chow and W. K. Chow, Trajectories of large respiratory droplets in indoor environment: A simplified approach, Building and Environment, 183 (2020), 107196 1-11.

[7] L. Evans, Partial Differential Equations, Second Edition, Americam Mathematical Society, Providence, Rhode Island, 2010.

[8] S. Evje, T. Flatten, On the wave structure of two-phase flow models, SIAM Journal on Applied Mathematics, 67 (2007), 487-511.

[9] R. C. Flagan, J. H. Seinfeld, Fundamentals of Air Pollution Engineering, 1988, Prentice Hall.
[10] S. Grossberg, D. S. Jarman, G. R. Tabor , Derivation of the Adjoint Drift Flux Equations for Multiphase Flow, Fluids, 5 (2020), 31.
[11] J. K. Gupta, C. H. Lin, and Q. Chen, Flow dynamics and characterization of a cough, Indoor Air, 19 (2009), 517-525.
[12] T. Hibiki, M. Ishii, Distribution parameter and drift velocity of drift-flux model in bubbly flow, International Journal of Heat and Mass Transfer, 45 (2002), 707-721.
[13] S. Holmberg, Y. Li, Modelling of the indoor environment-particle dispersion and deposition, Indoor Air, 8 (1998), 113-122.
[14] P. Katre, S. Banerjee, S. Balusamy, K. C. Sahu, Fluid dynamics of respiratory droplets in the context of COVID-19: airborne and surface borne transmissions Physics of Fluids, 33 (2021), 081302 11-19.
[15] S. Kumar and H. P. Lee, The perspective of fluid flow behavior of respiratory droplets and aerosols through the facemasks in context of SARS-CoV-2, Physics of Fluids, 32 (2020) 1-15.
[16] D. H. Morris, K. C. Yinda, A. Gamble, F. W. Rossine, Q. Huang, T. Bushmaker, R. J. Fischer, M. J. Matson, N. V. Doremalen, P. J. Vikesland, L. C. Marr, V. J. Munster, J. O. Lloyd-Smith, Mechanistic theory predicts the effects of temperature and humidity on inactivation of SARS-CoV-2 and other enveloped viruses, eLife 2021,10 (2021),e65902.
[17] S. Murakami, S. Kato, S. Nagano, Y. Tanaka, Diffusion characteristics of airborne particles with gravitational settling in a convection-dominant indoor flow field, Ashrae Transactions, 98 (1992), 82-97.
[18] R. R. Netz, Mechanisms of airborne infection via evaporating and sedimenting droplets produced by speaking, Journal of Physical Chemistry B, 124 (2020), 7093-7101.
[19] S. Paynter, Humidity and respiratory virus transmission in tropical and temperate settings, Epidemiology and Infection, 143 (2015), 1110-1118.
[20] M. R. Pendara and J. C. Páscoa, Numerical modeling of the distribution of virus carrying saliva droplets during sneeze and cough, Physics of Fluids, 32 (2020), 1-18.
[21] M. E. Rosti, M. Cavaiola, S. Olivieri, A. Seminara, and A. Mazzino, Turbulence role in the fate of virus-containing droplets in violent expiratory events, Physical Review Research, 3 (2021), 013091 1-10.
[22] V. Stadnytskyi, C. E. Bax, A. Bax and P. Anfinrud, The airborne lifetime of small speech droplets and their potential importance in SARS-CoV-2 transmission, Biological Sciences, 117 (2020), 11875-11877.
[23] H. Wang, Z. Li, X. Zhang, L. Zhu, Y. Liu and S. Wang, The motion of respiratory droplets produced by coughing, Physics of Fluids, 32 (2020), 125102, 1-14.
[24] L. Wessendorf, E. Richter, B. Schulte, R. M. Schmithausen, M. Exner, N. Lehmann, M. Coenen, C. Fuhrmann, A. Kellings, A. Husing, K.H. Jockel, H. Streeck, Dynamics, outcomes and prerequisites of the first SARS-CoV-2 superspreading event in Germany in February 2020: a cross-sectional epidemiological study. BMJ Journal Open, 12(4):e059809 (2022).
[25] X. Xie, Y. Li, H. Sun, L. Liu, Exhaled droplets due to talking and coughing, Journal of The Royal Society, 6 (2009), S703-S714.
[26] Y. Yang, W. Y. Chan, C. L. Wu, R. Y. C. Kong and A. C. K. Lai, Minimizing the exposure of airborne pathogens by upper-room ultraviolet germicidal irradiation: an experimental and numerical study, Journal of The Royal Society Interface, 9 (2012), 3184-3195.
[27] B.Zhao, Z. Zhang and X. Li, Numerical study of the transport of droplets or particles generated by respiratory system indoors, Building and Environment, 40 (2005), 1032-1039.

University of Coimbra, CMUC, Department of Mathematics, Coimbra, Portugal
E-mail address: ferreira@mat.uc.pt

P. de Oliveira
University of Coimbra, CMUC, Department of Mathematics, Coimbra, Portugal
E-mail address: poliveir@mat.uc.pt

P. Silva
Instituto Politécnico de Coimbra, ISEC, DFM, Rua Pedro Nunes, 3030-199 Coimbra, Portugal. CMUC.
E-mail address: pascals@isec.pt